# Experience-Shared Variable-Step Predictive Control of Range-Extended Electric Vehicles Using Transferable Driver Model

Ji Li, *Member, IEEE*, Zirui Li, *Student Member, IEEE*, Chengqing Wen, Yanhong Wu, Roger Dixon, Xiaosong Hu, *Fellow, IEEE*, and Hongming Xu

***Abstract*— Integrating range-extended electric vehicles (REEVs) in the automotive market is a key part of the drive toward environmental sustainability. This paper leverages an experience-shared approach to variable-step predictive control to improve REEV energy efficiency, where a transferable driver model is designed to accommodate varying driver experience levels via knowledge transfer. This model incorporates a confidence level factor to determine the effective length of speed prediction, ensuring a more accurate and reliable model predictive control system with lower requirement data. A grey wolf optimizer is employed as an advanced global solver in the model predictive control system of the studied REEV to seek better energy-saving performance. Experimental validation utilizes an industry-recognized driver-in-the-loop co-simulation platform to investigate the proposed approach's performance. Compared to Gaussian mixture regression one, the transferable driver model achieves a 27.29% improvement in speed prediction accuracy. Incorporating the driver model, the proposed experience-shared variable-step predictive control approach helps a 3.9% reduction in fuel consumption compared to an LQR-driven MPC one.**

***Index Terms*— Driver transferable model, driving simulator, inadequate observation, range-extended electric vehicles, variable-step model predictive control.**

## I. Introduction

As GLOBAL attention increasingly focuses on environmental sustainability and concerns over the depletion of fossil fuel reserves, finding sustainable transportation solutions has become a pressing priority. Hybrid electric vehicle (HEV) technology demonstrates immense potential in the development of sustainable transportation [1]. Range-extended electric vehicles (REEVs) propose an innovative solution by combining the low-emission benefits of electric generators with the extended range capabilities of auxiliary power sources like internal combustion engines (ICEs) [2] or fuel cells [3]. Therefore, an optimal energy management strategy is required to improve fuel economy [4] and emissions reduction [5] through efficient energy-flow allocations.

In HEV energy management, rule-based strategies are commonly used for their simplicity and ease of implementation. However, they are limited in their adaptability to changing conditions and may not always provide optimal performance [6]. The equivalent consumption minimization strategy optimizes energy usage by balancing fuel and battery consumption in real-time. It is crucial to calculate the equivalent factor to enhance the adaptive ability for different scenarios [7]. Fuzzy logic has been widely applied in the energy management of HEVs. However, these fuzzy logic-based approaches rely on human cognition and are limited by expert knowledge [8], [9]. Reinforcement learning has gained attention for its ability to adapt to dynamic environments through learning-based approaches, its training process is often computationally expensive and may struggle with real-time implementation in constrained systems [10]. Model predictive control (MPC) is widely recognized for its ability to predict state variables' trajectories and further optimize present actions for reaching predefined objectives [11]. Therefore, selecting the proper types of predictor and solver is the key to achieving optimal performance of HEV energy management. The linear quadratic regulator (LQR) solver is commonly used in the MPC of hybrid electric vehicles. The trajectory-tracking control of vehicles utilizes the LQR-driven MPC approach to minimize lateral tracking deviation while tracking the desired trajectory and speed [12]. Such a method requires a trial-and-error process to determine its parameters, but that could be time-consuming and fall into the local optimal [13].

Nature-inspired evolutionary algorithms could be ideal solvers used for the MPC framework that provided the exploration and exploitation capabilities for finding the global optimum. Research studies have demonstrated that tuning MPC using evolutionary algorithms can provide better performance than the LQR-driven MPC approach [14]. A study on traffic light optimization using genetic algorithms has shown the performance of the evolutionary optimization-driven MPC

Received 2 May 2024; revised 26 September 2024; accepted 27 October 2024. Date of publication 13 November 2024; date of current version 9 January 2025. The Associate Editor for this article was C. K. Sundarabalan. *(Corresponding authors: Zirui Li; Hongming Xu.)*

Ji Li, Chengqing Wen, Roger Dixon, and Hongming Xu are with the Department of Mechanical Engineering, University of Birmingham, B15 2TT Birmingham, U.K. (e-mail: j.li.1@bham.ac.uk; cxw053@student.bham.ac.uk; r.dixon@bham.ac.uk; h.m.x@bham.ac.uk).

Zirui Li is with the School of Mechanical Engineering, Beijing Institute of Technology, Beijing 100081, China, and also with the Chair of Traffic Process Automation, "Friedrich List" Faculty of Transport and Traffic Sciences, TU Dresden, 01069 Dresden, Germany (e-mail: z.li@bit.edu.cn).

Yanhong Wu is with the Department of Mechanical Engineering, University of Birmingham, B15 2TT Birmingham, U.K., and also with Tianjin Key Laboratory of Intelligent Unmanned Swarm Technology and System, School of Electrical and Information Engineering, Tianjin University, Tianjin 300072, China (e-mail: yxw1184@student.bham.ac.uk).

Xiaosong Hu is with the College of Mechanical and Vehicle Engineering, Chongqing University, Chongqing 400044, China (e-mail: xiaosonghu@ieee.org).

Digital Object Identifier 10.1109/TITS.2024.3489018

approach [15]. Li et al. applied chaos-enhanced accelerated particle swarm optimization (PSO)-driven MPC to power system control, demonstrating the effectiveness of PSO in improving MPC performance [16]. He et al. proposed an improved MPC-based energy management strategy using PSO to improve the accuracy of the predictor for mobile robot path planning that reduces path length and simulation time with faster convergence [17]. Grey wolf optimization (GWO) enables to balance of exploration and exploitation more efficiently, enhancing its optimization performance, compared to genetic algorithms [18], simulated annealing [19], and PSO [20], [21]. The GWO-driven MPC approach can improve the solver's effectiveness by considering the best three optimal positions in each iteration, thereby enhancing the global optimization search capability [22].

The predictor is another factor that helps guarantee the overall effectiveness of the MPC-based control system. Incorporating human driving preferences into speed prediction enhances prediction accuracy [23]. Driver predictive models can generally be achieved by rule-based and machine learning-based methods [24], [25], [26]. In terms of rule-based models, adaptation to various drivers typically involves manually adjusting the model's thresholds or parameters [27]. By continuously learning from real-time data, machine learning-based methods can effectively accommodate the unique patterns of individual drivers, but they heavily depend on the data itself [28]. Transfer learning can significantly enhance the performance of ML models by leveraging knowledge from pre-existing models [29], which is a potential solution to build prediction models with insufficient data [30], [31]. Hence, the authors believe that using transfer learning to address the limitations of driver modeling with insufficient data in MPC is a promising approach. Although the method is expected to improve the accuracy, there are still limitations caused by the data itself.

This paper proposes an experience-shared variable-step predictive control approach for REEVs to improve energy-saving performance while reducing the driver predictive model's sample size. Meanwhile, a new factor of confidence level is introduced and utilized to adjust the evaluation length of the speed prediction used in the proposal MPC approach. The three main contributions of this study are:

1) An experience-shared variable-step predictive control approach is proposed to improve control robustness by variable-step enhanced predictor;
2) A transferable driver model is developed to address the problem of accurate driver modeling in insufficient data conditions;
3) The potential of the proposed approach is validated using a driver-in-the-loop co-simulation between the cockpit driving simulator, IPG Carmaker, and the AVL CRUISE package.

After the problem is introduced (here in Section I), a well-sourced REEV system and its energy flow are analyzed in Section II. Section III elaborates on the design procedure of the transferable driver model with inadequate observation samples and an evolutionary MPC approach of variable-step predictive optimal control, where the GWO algorithm is developed to solve a multi-objective control problem in real time. In Section IV, the experimental setup, including data collection and validation scheme, is established. Section V presents a comprehensive comparative study in terms of transferable driver models, prediction steps, and control approaches. Finally, the conclusions are drawn in Section VI.

TABLE I
SPECIFICATION OF THE STUDIED REEV

| Parameters | Value | Unit |
|---|---|---|
| Vehicle Mass | 1700 | $kg$ |
| Frontal Area | 1.97 | $m^2$ |
| Max.Engine Torque | 263.83 | $Nm$ |
| Max.Engine Speed | 7500 | $rpm$ |
| Max.generator Power | 102 | $kW$ |
| Max.generator Torque | 345.6 | $Nm$ |
| Max.Generator Torque | 239 | $Nm$ |
| Battery Capacity | 10 | $Ah$ |

## II. PROBLEM STATEMENT

This Section provides a detailed overview of the studied REEV model, including its configuration and energy flow dynamics. The energy management strategy is designed to control the power output of the ICE to control the energy distribution between the ICE and the battery, aiming to maintain SOC stability while minimizing fuel consumption in charge-sustaining mode. The system's state equations are derived from the REEV dynamics model, which explicitly defines the control variables, state variables, and output variables, ensuring a clear representation of the energy flow and interactions between the battery and engine.

### A. REEV Configuration

The REEV configuration comprises three integral segments: propulsion, charging, and energy storage. The propulsion subsystem comprises a traction electric generator and a transmission system responsible for propelling the vehicle. The traction electric generator derives power from a battery pack organized in a 120s2p configuration (120 cells in series and 2 in parallel), serving as the primary energy storage unit. Concurrently, the charging of the battery pack is facilitated through a generator actuated by an ICE. The dataset employed in this study is sourced from AVL CRUISE, with detailed parameters provided in Table I.

### B. Energy Flow of the Studied REEV

To determine the energy flow of the REEV, a commonly used longitudinal dynamics model is applied here. The required traction force $F_{\text{trac},k}$ is equate to the combination of acceleration resistance $F_{\text{acce,k}}$, aerodynamic resistance $F_{\text{aero},k}$, rolling resistance $F_{\text{roll},k}$, and grade resistance $F_{\text{grad},k}$. It can be written as:

$$F_{\text{trac},k} = F_{\text{acce},k} + F_{\text{aero},k} + F_{\text{roll},k} + F_{\text{grad},k} \tag{1}$$

in which

$$\begin{cases} F_{\text{acce},k} = m \cdot a_k \\ F_{\text{aero},k} = \dfrac{1}{2}\rho \cdot C_d \cdot A_f \cdot v_k^2 \\ F_{\text{roll},k} = C_r \cdot m \cdot g \cdot \cos(\theta_k) \\ F_{\text{grad},k} = m \cdot g \cdot \sin(\theta_k) \end{cases} \tag{2}$$

where $k$ is the discrete-time point; $m$ is the mass of the vehicle; $a_k$ is the acceleration of the vehicle; $\rho$ is the density of air; $C_d$ is the drag coefficient; $A_f$ is the frontal area of the vehicle; $v_k$ is the speed of the REEV; $C_r$ is the rolling resistance coefficient, which quantifies the resistance to rolling on a surface; $g$ is the acceleration due to gravity; $\theta_k$ is the slope grade angle. Then, the wheel torque $T_{\text{wheel},k}$ and wheel speed $n_{\text{wheel},k}$, are derived from the traction force by:

$$\begin{cases} n_{\text{wheel},k} = \dfrac{v_k}{R_{\text{wheel}}} \\ T_{\text{wheel},k} = F_{\text{trac},k} \cdot R_{\text{wheel}} \end{cases} \tag{3}$$

where $R_{\text{wheel}}$ is the wheel radius. Then, the electric traction motors are informed by the wheel dynamics. Considering the torque and power limitation of the motor under a certain motor speed, the traction motor speed $n_{\text{mot},t}$ and torque $T_{\text{mot},k}$ can be described as following equations.

$$\begin{cases} n_{\text{mot},k} = n_{\text{wheel},k} \cdot i_{\text{tran}} \\ T_{\text{mot},k} = \dfrac{T_{\text{wheel},k}}{i_{\text{tran}} \cdot \eta_{\text{tran}}} \end{cases} \tag{4}$$

where $i_{\text{trans}}$ is the total transmission ratio from the motor to the wheel; $\eta_{\text{tran}}$ is the efficiency of the transmission system. Then the power of the traction motor can be written as:

$$P_{\text{mot},k} = T_{\text{mot},k} \cdot n_{\text{mot},k} \cdot \eta_{\text{mot}} \tag{5}$$

where $\eta_{\text{mot}}$ is the efficiency of motor. The traction motor is powered by the battery pack, whose state of charge (SOC) is influenced by the power from both the electric traction motor $P_{\text{mot},k}$ and the generator $P_{\text{gen},k}$, which can be written as:

$$P_{\text{bat},k} = P_{\text{mot},k} + P_{\text{gen},k} \tag{6}$$

The battery can be modeled as the internal resistance model. According to Kirchhoff's law of closed-loop circuit, the battery current $I_{\text{bat},k}$ can be calculated using the equation:

$$I_{\text{bat},k} = \frac{V_{oc} - \sqrt{V_{oc}^2 - 4R_{\text{int}} \cdot P_{\text{bat},k}}}{2R_{\text{int}}} \tag{7}$$

where, $V_{oc}$ is the voltage of open circuit; $R_{\text{int}}$ is the internal resistance; $P_{\text{bat},k}$ is the required power. The output power of the generator $P_{\text{gen},k}$ is:

$$P_{\text{gen},k} = T_{\text{ice},k} \cdot n_{\text{ice},k} \cdot \eta_{\text{gen}} \tag{8}$$

where $T_{\text{ice},k}$ is the engine torque, $n_{\text{ice},k}$ means the engine rotational speed, and $\eta_{\text{gen}}$ is the efficiency of the generator.

So far, the REEV model can be rewritten as a nonlinear system model:

$$\begin{cases} x_{k+1} = f(x_k, u_k) \\ y_k = C x_k \end{cases} \tag{9}$$

where $C$ denotes the identity matrix, $x_k$ denotes the state vector, $u_k$ denotes the control vector, and $y_k$ denotes the output vector of the REEV model, and they are defined as follows.

$$\begin{cases} x_k = [\text{SOC}_k, \text{E}_k]^\top \\ u_k = P_{\text{gen},k} \end{cases} \tag{10}$$

where $\text{SOC}_k$ can be calculated using the equation:

$$\text{SOC}_\text{k} = \text{SOC}_{\text{k}_0} + \frac{1}{Q_{\max}} \sum_{k=1}^{N} I_{\text{bat},k} \tag{11}$$

where $\text{SOC}_{\text{k}_0}$ is the initial state of charge, $I_{\text{bat},k}$ is the battery current during the time step, and $Q_{max}$ is the maximum capacity of the battery. $E_k$ is the total fuel consumption, which is obtained by integrating the fuel consumption rate $\dot{m}_{f,k}$:

$$E_k = \sum_{k=1}^{N} \dot{m}_{f,k} \tag{12}$$

## III. Experience-Shared Variable-Step Predictive Control Apporach

To improve energy-saving performance while reducing the driver predictive model's sample size, this paper proposes an experience-shared variable-step prediction control approach for REEVs. As shown in Fig.1, the transferable driver model comprises three distinct components: dynamic time warping, Procrustes analysis, and Gaussian mixture model-Gaussian mixture regression (GMM-GMR). Considering the variability in driving behaviors, the experience-sharing mechanism leverages the distribution characteristics of drivers in the source domain and a limited number of samples from the target domain to fully represent the driving features of drivers in the target domain. In data-driven driver behavior modeling, the purpose of establishing a transferable model is to find the samples in the source domain that can be used for modeling in the target domain, to expand the dataset of the target domain, and ultimately solve the problem of modeling new drivers under data sparse conditions. The results of the transferable model are used as the predictive speed for MPC, in which the confidence level is used to adjust the evaluation length of the speed prediction. The evolutionary algorithm, i.e., the GWO algorithm, is applied to prevent the solver from falling into local optima.

### A. Source to Target Domain Mapping

The dynamic time warping initially emerged for aligning two temporal trajectories by determining an optimal "warping path" through dynamic programming [32]. The cost function minimizes the distance between corresponding sample points, typically measured using the Euclidean distance. In driver behavior transfer learning, dynamic time warping identifies corresponding points in steering wheel angle change trajectories between a source and a target driver. The warping path ensures each target domain sample point aligns with at least one source domain point. This path, represented as a matrix $\mathbf{w}$, delineates the corresponding points between drivers. Once a warping path is established between a source and a target

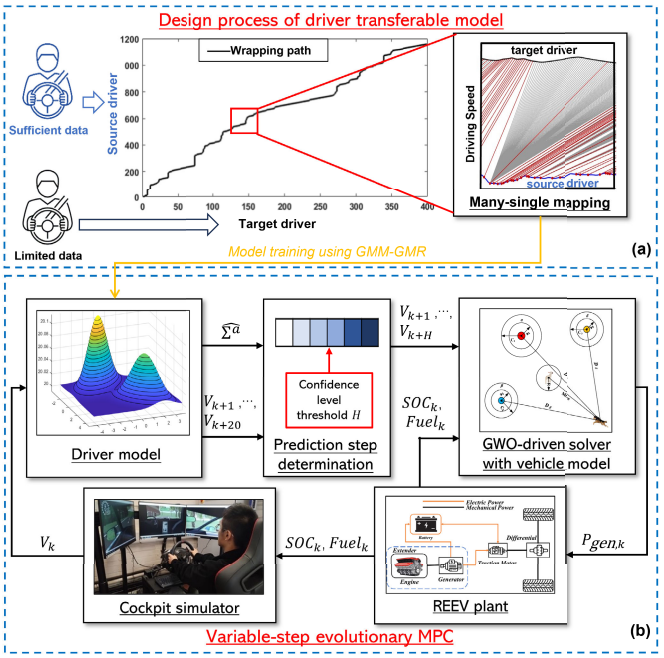


Fig. 1. The illustration of experience-shared variable-step predictive control using transferable driver model: a) design process of transferable driver model; and b) workflow of variable-step evolutionary MPC.

driver, the corresponding points along this path are distinctly defined and can be encapsulated in a Boolean matrix denoted as $\mathbf{W}$, which only includes 0 and 1 for corresponding pairing.

$$\mathbf{W} = \begin{bmatrix} w_{11} & \cdots & w_{1N_{ta}} \\ \vdots & \ddots & \vdots \\ w_{N_s1} & \cdots & w_{N_sN_{ta}} \end{bmatrix} \tag{13}$$

where each element $w = (i, j)$ constitutes an index pair, it means $i^{th}$ sample from the source driver's data is corresponding to $j^{th}$ sample from the target driver's data. Consequently, the warping path can be formally defined as:

$$\mathbf{w} = (w_1, w_2, \ldots, w_L) \tag{14}$$

where $L$ is the length of the warping path and $w_l \in \mathbf{W}$, with $l$ equates to $1, 2, \ldots, L$. To determine the warping path, a commonly utilized approach is to minimize the similarity cost function. The extended feature from source and target drivers are defined as $\mathbf{Z}^{ta}$ and $\mathbf{Z}^{so}$, which is the concatenation of input feature and prediction label. It will be clearly defined in the experimental setup. The similarity cost function employed by dynamic time warping can be defined as

$$J(w_l) = \sum_{t=l}^{L} \left\| \mathbf{Z}^{ta}_{w_k} - \mathbf{Z}^{so}_{w_k} \right\|^2 \tag{15}$$

where $\|\cdot\|$ is the Euclidean norm. An effective dynamic time warping must meet three conditions: boundary condition, monotonicity condition, and step-size condition [32]. Under the aforementioned constraints, the optimal warping path can be iteratively solved using the dynamic programming method. The Bellman equation utilized in the dynamic programming approach is as follows:

$$\begin{aligned} w_l^* &= \arg\min_{w \in W} \sum_{k=l}^{L} \left\| \mathbf{Z}^{ta}_{w_k} - \mathbf{Z}^{so}_{w_k} \right\|^2 \\ &= \arg\min_{w \in W} \left( \left\| \mathbf{Z}^{ta}_{w_l} - \mathbf{Z}^{so}_{w_l} \right\|^2 + J(w_{l+1}) \right) \end{aligned} \tag{16}$$

where $l$ and $l+1$ are adjacent index pairs.

### B. Driver Experience Sharing

To solve the problem of insufficient data in the target domain, our goal is to expand the target dataset. The additional samples come from the transformation of samples in the source domain. The specific transformation matrix can be obtained by the corresponding wrapping path identified through the dynamic time warping. Given a source domain dataset $\mathbf{Z}^{so}$ and a target domain dataset $\mathbf{Z}^{ta}$, Procrustes analysis facilitates this transfer via a linear transformation [33]. The local linear mapping relationship is formally characterized as a transformation matrix from the source domain to the target domain. This Procrustes analysis process can be articulated as follows:

$$\mathbf{Q}^* = \left( \Sigma^{so,so} \right)^{-1} \Sigma^{ta,so} \tag{17}$$

$\Sigma^{so,so}$ and $\Sigma^{ta,so}$ are covariance matrices:

$$\Sigma^{so,so} = \frac{1}{N^{ta}} \sum_{i=1}^{N^{ta}} (\mathbf{Z}^{so}_i - \bar{\mathbf{Z}}^{so})(\mathbf{Z}^{so}_i - \bar{\mathbf{Z}}^{so})^\top \tag{18}$$

$$\Sigma^{ta,so} = \frac{1}{N^{ta}} \sum_{j=1}^{N^{ta}} (\mathbf{Z}^{ta}_j - \bar{\mathbf{Z}}^{ta})(\mathbf{Z}^{so}_j - \bar{\mathbf{Z}}^{so})^\top \tag{19}$$

where $\bar{\mathbf{Z}}^{so}$ and $\bar{\mathbf{Z}}^{ta}$ are means of $\mathbf{Z}^{so}$ and $\mathbf{Z}^{ta}$. After the linear transformation of PA, $Z$ for GMM-GMR can be written as:

$$\mathbf{Z} = [\mathbf{Q}^* \mathbf{Z}^{so}, \mathbf{Z}^{ta}] \tag{20}$$

### C. Driver Behavior Modeling

A GMM is a probabilistic model that assumes data is generated from a mixture of several Gaussian distributions, each with its mean and variance [34]. It's used for applications like clustering and pattern recognition, where data exhibits multi-modal characteristics. In a multi-dimensional space with multiple random variables, the probability density function of the multi-dimensional Gaussian distribution takes the form:

$$\begin{aligned} p(\mathbf{z}|\pi_{1:H}, \mu_{1:H}, \Sigma_{1:H}) &= \sum_{h=1}^{H} \pi_h \mathcal{N}(\mathbf{z}|\mu_h, \Sigma_h) \\ &= \sum_{h=1}^{H} \frac{\pi_h}{(2\pi)^{D/2} |\Sigma_h|^{1/2}} \\ &\quad \times \exp\left( -\frac{1}{2} (\mathbf{z} - \mu_h)^T \Sigma_h^{-1} (\mathbf{z} - \mu_h) \right) \end{aligned} \tag{21}$$

where each Gaussian distribution is referred to as a Gaussian component. $H \in \digamma$ is the number of components. $\mu_h$ and $\Sigma_h$ are the mean and variance of $h^{th}$ Gaussian distribution. $\pi_h \in (0, 1)$ is the weight of $h^{th}$ Gaussian distribution with

$\sum_{k=1}^{K} \pi_k = 1$. The parameter identification of the GMM can be accomplished through the Expectation-Maximization algorithm. The final model parameters $\Theta$ are represented as follows:

$$\Theta = \{\pi_h, \mu_h, \Sigma_h\}_{h=1}^{H} \tag{22}$$

The GMM obtained from training with observed samples is denoted as:

$$p(\mathbf{Z}_k|\Theta) = \sum_{h=1}^{H} \pi_h \mathcal{N}(\mathbf{Z}_k|\mu_h, \Sigma_h) \tag{23}$$

where $\mu_h$ and $\Sigma_h$ can be expressed as:

$$\mu_h = \begin{bmatrix} \mu_h^s \\ \mu_h^a \end{bmatrix} \tag{24}$$

$$\Sigma_h = \begin{bmatrix} \Sigma_h^s & \Sigma_h^{sa} \\ \Sigma_h^{as} & \Sigma_h^a \end{bmatrix} \tag{25}$$

At time $k$, given the input state feature $\mathbf{Z}_k$, the GMR can calculate the output $a_k$ based on the parameters of the GMM. For each component $h$, the inferring process is formulated as follows:

$$\hat{\mu}_h^a = \mu_h^a + \Sigma_h^{as} \left(\Sigma_h^{ss}\right)^{-1} \left(\mathbf{Z}_k - \mu_h^s\right) \tag{26}$$

$$\hat{\Sigma}_h^a = \Sigma_h^a - \Sigma_h^{as} (\Sigma_h^s)^{-1} \Sigma_h^{sa} \tag{27}$$

The output mean $\hat{\mu}^a$ and uncertainty $\hat{\Sigma}^a$ is the aggregation of all $h$ GMM components,

$$h_h = \frac{\pi_h \mathcal{N}(\mathbf{Z}_k|\mu_h^s, \Sigma_h^s)}{\sum_{j=1}^{H} \pi_j \mathcal{N}(\mathbf{Z}_k|\mu_j^s, \Sigma_j^s)} \tag{28}$$

$$\hat{\mu}^a = \sum_{h=1}^{H} h_h \hat{\mu}_h^a(\mathbf{Z}_k) \tag{29}$$

$$\hat{\Sigma}^a = \sum_{h=1}^{H} w_h \hat{\Sigma}_h^a(\mathbf{Z}_k) \tag{30}$$

where $w_h$ is the weight of each component. The uncertainty $\hat{\Sigma}^a$ can be served as the confidence level for the downstream task. In the multi-step prediction, all predicted uncertainties in the future steps are normalized to (0, 1).

### D. Variable-Setp Evolutionary MPC

To prevent the solver of MPC from falling into local optima, a nature-inspired evolutionary algorithm GWO is applied here. The GWO algorithm has emerged as a nature-inspired metaheuristic algorithm that demonstrates distinctive efficacy in addressing the global optimization issue [20]. GWO should maintain diversity within the solution space by emulating the collaborative and individualistic tendencies of grey wolves. To optimize the energy management between SOC and fuel consumption, the optimal output power of ICE is searched by GWO based on the predicted speed. To handle the difficulty of the timeliness of rolling optimization for the MPC approach, the REEV system model, Eq. (9), can be defined as:

$$x_{k+1} = f(x_k, u_k) \tag{31}$$

The objective cost function defined with consideration of SOC and fuel consumption can be defined as:

$$J_k = J_1 \cdot \frac{1}{J_1{}^*} \cdot \frac{1}{J_{1,\max}} + J_2 \cdot \frac{1}{J_2{}^*} \cdot \frac{1}{J_{2,\max}} \tag{32}$$

where $J_{1,\max}$ and $J_{2,\max}$ are the maximum value used for normalization; $J_1{}^*$ and $J_2{}^*$ are scaling coefficients of optimization targets $J_1$ and $J_2$, which are defined as:

$$\begin{cases} J_1 = \sum_{k=1}^{k=N} E_{\mathrm{k}} \\ J_2 = \sum_{k=1}^{k=N} \left(|\mathrm{SOC_{k\text{-}1}} - \mathrm{SOC}_k|\right) \end{cases} \tag{33}$$

where $N$ is the length of the predicted speed.

Furthermore, the MPC approach offers a significant benefit in effectively addressing operational constraints of the cost function, as pointed out in [35], which can be written as:

$$\begin{cases} x_{\min} \le x_k \le x_{\max} \\ u_{\min} \le u_k \le u_{\max} \end{cases} \tag{34}$$

where $x_k$ and $u_k$ are defined in Eq. (13). Here, $x_{\min}$ and $x_{\max}$ is the matrix of SOC and fuel consumption, which are $[0.67, 0]^\top$ and $[0.68, 7.26]^\top$. The maximum fuel consumption is calculated based on the maximum output power of ICE of the studied REEV. Next, the cumulative cost function with the prediction sequence undergoes optimization by applying the GWO algorithm. GWO algorithm is a recognized optimization technique inspired by the social behavior of wolves [36], [37].

By simulating both collaborative and solitary behaviors inherent in grey wolves, the GWO algorithm ensures the preservation of a diverse set of solution possibilities within the optimization problem. Consequently, the cost function, Eq. (32), is effectively addressed by applying the GWO method.

## IV. Experimental Set-up

To evaluate the proposed experience-shared variable-step predictive control approach, a driving cockpit simulator with IPG Carmaker is established. Five different drivers are invited to do a virtual driving. The validation procedure is designed and dedicated to testing the proposed approach's effectiveness on a REEV in different scenarios.

### A. Data Collection and Profile

Thrustmaster T500RS consists of a steering wheel and pedals with force feedback. The pedal position and steering wheel angle signals are sent via USB 3.0 to the IPG Carmaker installed on the host PC, which then displays the driving scenario on monitors. This cockpit simulator is used to realize the driver's interaction with the virtual driving scenarios built in the IPG Carmaker. The scenario consists of a two-way single-lane road with flat, uphill, downhill, curved, and straight roads with traffic. A REEV with an automatic gearbox is selected as the vehicle and five drivers are invited to drive an identical test track. The collection process of the driving profile is shown in Fig. 2.

The drivers were exposed to identical driving conditions and were expected to conform to the speed limits as well as other driving laws. The speed limit varied along the test

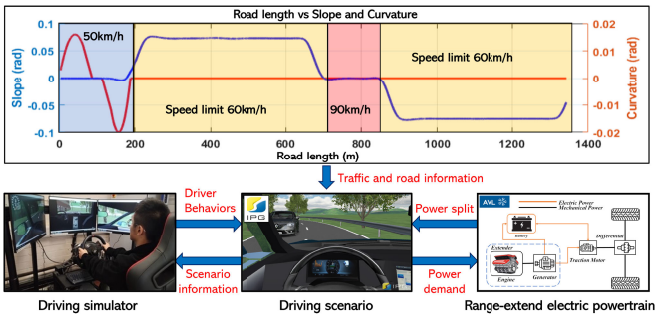


Fig. 2. Data collection process of using drver-in-the-loop co-simulation platform.

TABLE II
INFORMATION OF HUMAN DRIVER PARTICIPANTS

| Driver # | Age | Time to hold a driving license | Annual mileage (mile) |
|---|---|---|---|
| 1 | 31 | 14 | 2000 |
| 2 | 31 | 10 | 3000 |
| 3 | 28 | 11 | 2500 |
| 4 | 30 | 14 | 1500 |
| 5 | 30 | 8 | 6000 |

track, with speed limits in different scenarios. The speed limit is 50 km/h on uphill and downhill sections, 60 km/h on flat curved sections, and 90 km/h on flat straight lines. The information on the five drivers is shown in Table II.

The measured variables during the simulator testing are as follows: vehicle speed, $v$, wheel steering angle, $\delta$, gas pedal position, $P_{\text{gas}}$, and brake pedal position, $P_{\text{brake}}$. These measured variables were recorded with a 10 Hz sampling frequency across a 10-minute testing period, thus leading to 6000 measured points per driver, totaling 30000 samples.

### B. Validation Procedure

The validation procedure is carefully designed to systematically evaluate the proposed MPC approach. Section III presents the general formulation for transferable driver modeling, where the extended features of driver behavior are formulated as $\mathbf{z}_k = [\mathbf{s}_k, \mathbf{a}_k]$. Considering that driving speed is a continuously changing process, $\mathbf{s}_k$ is defined as the vehicle state and driver control information over the past $N_{past}$ time steps $\mathbf{s}_k = [\mathbf{X}_{k-N_{past}+1}, \ldots, \mathbf{X}_k]$. Similarly, $\mathbf{a}_k = \mathbf{X}_{k+1}$. Based on the features collected during the data acquisition process, $\mathbf{X} = [v, P_{\text{gas}}, P_{\text{brake}}, \delta]$, where $v$ denotes vehicle speed, $P_{\text{gas}}$ denotes gas pedal position, $P_{\text{brake}}$ denotes brake pedal position, and $\delta$ denotes wheel steering angle. To generate multi-step predictions about future driving speeds, a rolling prediction strategy is adopted. It first predicts $\mathbf{a}_k$, then recombines past $N_{past} - 1$ time-steps' features $\mathbf{s}_{k+1}$. And so forth, the model achieves rolling prediction. Simultaneously, to streamline the model training process, the collected data underwent downsampling into 2 Hz as commonly used in most cases.

## V. RESULTS AND DISCUSSION

A thorough comparative study is conducted to evaluate the efficacy of the experience-shared variable-step predictive control approach. First, the transferable driver model undergoes testing to validate its effectiveness. Secondly, the impact of the MPC approach is scrutinized in-depth under both fixed prediction step and variable-step prediction conditions. Finally, a robustness analysis is carried out among the LQR-driven MPC, PSO-driven MPC, and GWO-driven MPC.

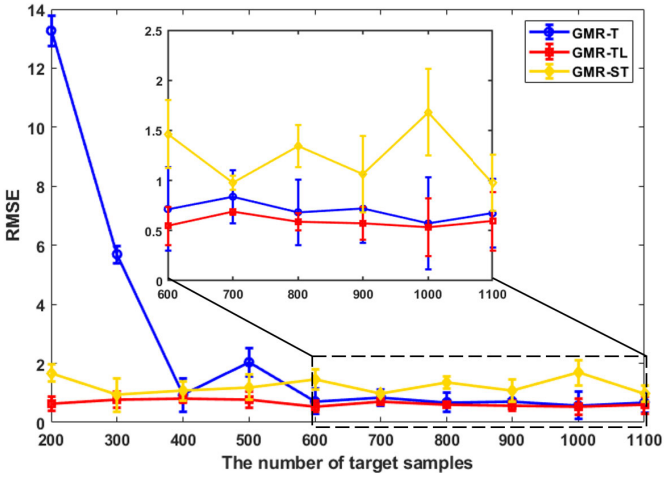


Fig. 3. The result of the variation of target sample sizes. Driver 1 is the source driver and Driver 4 is the target driver. The RMSE is the difference between prediction from the model and ground truth from the collected demonstration.

### A. The Performance of Transferable Driver Model

After the initial dynamic time warping process, the established warping path records index pairs between the source and target drivers, signifying correspondences. Due to sample quantity discrepancies, most target samples correspond to multiple source samples. This study adopts the midpoint of the sequence as the corresponding point for source-driving data. Subsequently, this result undergoes sample transfer via PA. The proposed transferable driver model is compared with two other methods: GMR-ST and GMR-S. GMR-S means training the model on the source driver's data and testing it on the target driver's data, while GMR-ST means training on a mix of sample source driver data and a smaller amount of target driver data. Twenty experimental groups were conducted, with five drivers alternately serving as source and target drivers. Table III depicts changes in prediction accuracy (RMSE) for each method in each experiment group, considering variations in the amount of data from the target driver.

The observed trend indicates a decrease in prediction error for all models as the volume of data increases. This underscores that, for driver learning models utilizing statistical learning methods, an augmentation in data volume substantially improves model performance, as illustrated in Fig. 3. Secondly, in any experiment transitioning from a source driver to a target driver, the model based on transfer learning methods consistently outperforms the other two baseline methods. This signifies that the transfer learning approach proposed in this paper enhances model performance, especially when the data volume for the target driver is small, showcasing a significant performance gap compared to non-transfer methods. As the data volume increases, the performance gap gradually diminishes. Thirdly, for the two non-transfer methods, it is

TABLE III
THE RMSE OF USING THREE TRANSFER METHODS WITH DIFFERENT SAMPLE SIZES

| Source → Target | 200 | | | 500 | | | 800 | | | 1100 | | |
|---|---|---|---|---|---|---|---|---|---|---|---|---|
| | **GMR-T** | **GMR-ST** | **TL** | **GMR-T** | **GMR-ST** | **TL** | **GMR-T** | **GMR-ST** | **TL** | **GMR-T** | **GMR-ST** | **TL** |
| Driver 1 → Driver 2 | 30.1 | 8.51 | 5.94 | 4.77 | 4.37 | 1.82 | 7.09 | 4.97 | 2.29 | 2.36 | 3.53 | 1.26 |
| Driver 1 → Driver 3 | 21.3 | 4.49 | 2.11 | 4.27 | 2.83 | 1.58 | 2.32 | 2.19 | 1.60 | 1.33 | 1.45 | 1.13 |
| Driver 1 → Driver 4 | 16.1 | 11.7 | 2.07 | 5.83 | 6.88 | 2.48 | 2.11 | 1.82 | 1.30 | 2.02 | 1.34 | 2.27 |
| Driver 1 → Driver 5 | 3.38 | 0.71 | 0.61 | 1.03 | 0.88 | 0.65 | 0.80 | 1.09 | 0.67 | 0.74 | 0.90 | 0.55 |
| Driver 2 → Driver 1 | 78.9 | 5.40 | 3.90 | 7.06 | 6.64 | 1.68 | 5.47 | 5.39 | 2.58 | 5.12 | 11.4 | 2.06 |
| Driver 2 → Driver 3 | 3.6 | 4.13 | 3.71 | 2.28 | 1.60 | 1.43 | 2.01 | 1.43 | 1.16 | 1.25 | 1.35 | 0.86 |
| Driver 2 → Driver 4 | 21.3 | 5.54 | 4.22 | 2.28 | 1.99 | 1.57 | 2.43 | 1.57 | 1.32 | 1.71 | 1.24 | 1.13 |
| Driver 2 → Driver 5 | 5.69 | 0.93 | 0.77 | 2.03 | 1.19 | 0.78 | 0.83 | 0.97 | 0.68 | 0.71 | 1.06 | 0.57 |
| Driver 3 → Driver 2 | 68.2 | 9.85 | 9.64 | 21.1 | 2.21 | 1.77 | 7.34 | 1.89 | 1.68 | 2.37 | 1.76 | 1.66 |
| Driver 3 → Driver 2 | 36.1 | 1.73 | 1.25 | 14.4 | 2.04 | 1.46 | 4.01 | 1.41 | 1.28 | 2.66 | 1.92 | 1.84 |
| Driver 3 → Driver 2 | 27.3 | 4.91 | 3.65 | 1.76 | 1.07 | 1.05 | 2.60 | 1.07 | 0.90 | 1.74 | 1.38 | 1.33 |
| Driver 3 → Driver 2 | 3.22 | 1.47 | 1.06 | 0.83 | 0.76 | 0.67 | 0.74 | 0.56 | 0.53 | 0.80 | 0.86 | 0.71 |
| Driver 4 → Driver 1 | 81.0 | 11.1 | 3.39 | 13.1 | 23.1 | 10.8 | 13.5 | 4.5 | 2.72 | 8.34 | 8.01 | 2.67 |
| Driver 4 → Driver 2 | 44.8 | 1.45 | 1.36 | 5.85 | 1.59 | 1.53 | 2.53 | 1.98 | 1.75 | 1.43 | 1.52 | 1.15 |
| Driver 4 → Driver 3 | 18.5 | 1.60 | 1.55 | 3.56 | 1.74 | 1.64 | 1.58 | 1.69 | 1.40 | 1.30 | 2.19 | 1.25 |
| Driver 4 → Driver 5 | 2.71 | 1.35 | 0.82 | 1.55 | 1.04 | 1.00 | 0.93 | 0.99 | 0.89 | 0.89 | 0.82 | 0.63 |
| Driver 5 → Driver 1 | 72.0 | 10.3 | 9.78 | 37.2 | 9.68 | 2.42 | 6.72 | 1.80 | 1.60 | 1.48 | 1.81 | 1.07 |
| Driver 5 → Driver 2 | 39.4 | 4.19 | 2.39 | 7.47 | 3.06 | 2.67 | 3.02 | 5.06 | 2.69 | 2.74 | 4.43 | 1.88 |
| Driver 5 → Driver 3 | 9.03 | 2.22 | 2.10 | 2.27 | 1.94 | 1.54 | 2.51 | 2.24 | 1.62 | 1.60 | 2.03 | 1.29 |
| Driver 5 → Driver 4 | 5.45 | 1.91 | 1.32 | 3.71 | 2.15 | 1.68 | 2.98 | 1.82 | 1.47 | 2.20 | 2.74 | 1.43 |
| Overall | 29.4 | 4.82 | 3.08 | 7.12 | 3.84 | 2.06 | 3.58 | 2.22 | 1.51 | 2.11 | 2.89 | 1.34 |

Note: GMR: Gaussian mixture regression; T: using target data; ST: using both source and target data; TL: transfer learning

TABLE IV
RESULTS OF USING THREE TRANSFER METHODS

| Transfer methods | Maximum MAE | Average MAE | Average RMSE |
|---|---|---|---|
| GMR-T | 17.78 | 0.83 | 1.678 |
| TL | 7.79 | 0.78 | 1.22 |
| GMR-ST | 15.99 | 0.85 | 1.54 |

observed that the driver model incorporating data from the target driver exhibits a smaller error. This implies that a model trained on one driver should not be universally applied to all other drivers for personalized driver modeling. Collecting new data for a different driver contributes to enhancing prediction performance.

In the approach delineated in this paper, the objective of multi-step driver prediction is its application in downstream energy management tasks. Fig. 4 depicts the predicted driving speed for the next 2 seconds in a 600-second driving cycle, comparing three methods. The detailed information is shown in Table IV. The results show that using transfer learning has the lowest maximum mean absolute error (MAE), average MAE, and average root mean square error (RMSE), therefore it is selected using in velocity predictor.

### *B. Fixed-Step Vs Variable-Step in MPC*

Based on the results of the transferable driver model, the predicted speed is utilized in the proposed MPC approach. In this approach, the length of the prediction step is determined by the confidence level, as defined in Eq. (30). Fig. 5 illustrates the mapping relationship between the confidence levels and the prediction steps, and further impact on the studied REEV. The color bar shows the value of the confidence level, which serves as the threshold for determining the number of prediction steps. The yellow color represents the highest confidence level with 20 prediction steps, while deep blue indicates the lowest confidence with non-prediction approach which means solving in real time using only the speed at the current time. This adaptive approach aims to optimize performance over time by adjusting prediction steps according to the confidence level. It should be noted that the prediction step length does not directly correlate with fuel efficiency at each time step.

Fig. 6 observes the impact of different prediction steps on the REEV's performance using the proposed MPC approach. Without prediction, the REEV using the proposed MPC approach cannot maintain the target SOC level, resulting in the highest instability. In contrast, the variable-step MPC approach demonstrates the least variance in SOC, suggesting a more stable performance. This reduced variability is achieved by evaluating driver behavior and adjusting the prediction steps in real time. It helps stabilize the SOC within the desired level.

Fig. 7 illustrates the statistical distribution of SOC and fuel consumption across different prediction steps in charge-sustaining mode. To observe the performance, the equivalent prediction step (fixed to 9) is the mean value of the variable prediction step. Compared to fixed-step ones, the variable-step MPC approach helps the REEV system achieve the least variation in SOC. The result shows that with 15 prediction steps is 4.94% higher than that with non-prediction and 0.27% higher than that with 10 steps.

### *C. Vehicle System Robustness of Using Different MPC Approaches*

The effectiveness of optimization solvers is paramount for achieving desired system performance. This study quantitatively compares the LQR-driven, PSO-driven, and GWO-driven MPC approach. Firstly, because the fitness value of LQR-driven MPC is a constant, therefore only PSO-driven and GWO-driven MPC is compared in Fig. 8. The real-time fitness refers to the cost function value calculated by iterations at each time step. To show the computational efficiency of algorithms, the maximum number of iterations for PSO and GWO is set to 100 and the number of agents is set to 5.

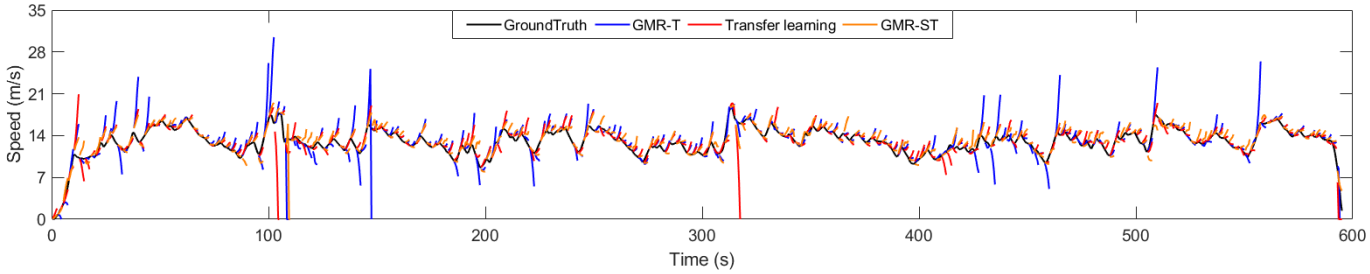


Fig. 4. The prediction results using three transfer methods based on the GMR model.

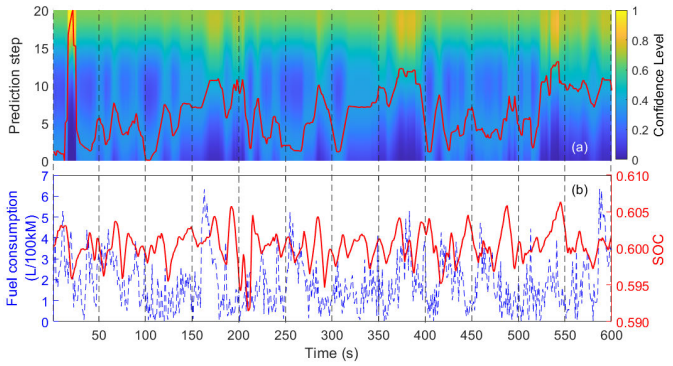


Fig. 5. The real-time performance of the studied REEV: a) prediction step and the confidence level; and b) fuel consumption and SOC.

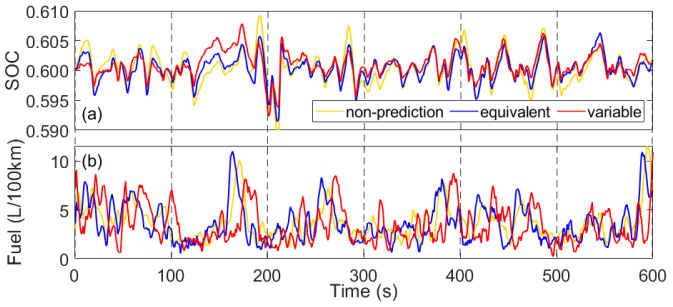


Fig. 6. Real-time performance under three different prediction steps: a) SOC; and b) fuel consumption.

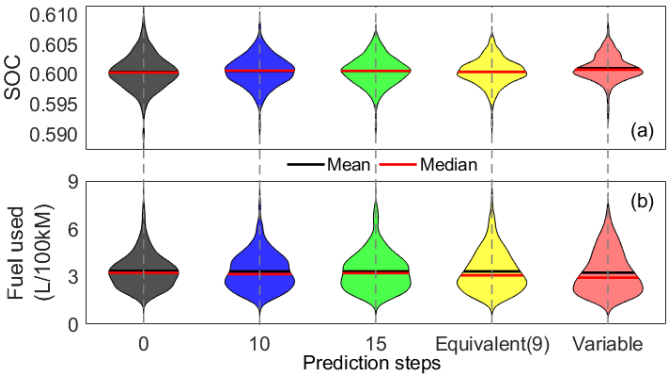


Fig. 7. Statistical results with various prediction steps: a) distribution of SOC's value; and b) distribution of fuel consumption.

It can be seen that the mean value of cumulative mean fitness by using PSO as the solver in the MPC framework is lower than that of using GWO until 7s, which may be due to GWO having a larger initial random value in the first second. However, after that, it is clear that the fitness value of using GWO as the solver is significantly smaller. The cumulative mean fitness by using GWO is 0.52% lower than using PSO. The result demonstrates that the GWO has the ability to achieve convergence within 20 iterations at each time step.

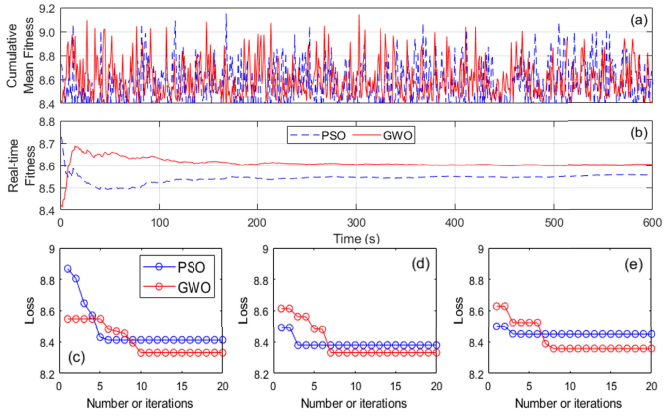


Fig. 8. Real-time fitness solved by PSO-driven and GWO-driven MPC approaches: a) cumulative mean fitness; b) real-time fitness by PSO and GWO; c) convergence curve in 7 s; d) convergence curve in 300 s; and e) convergence curve in 500 s.

TABLE V
PERFORMANCE COMPARISON OF USING DIFFERENT SOLVERS IN MPC

| Prediction step | Solver | Variance of SOC ($\times 10^{-6}$) | Fuel used (L/100kM) | Fuel saving |
|---|---|---|---|---|
| None | LQR | 3.43 | 3.56 | - |
| | PSO | 2.82 | 3.54 | 0.56% |
| | GWO | 2.82 | 3.53 | 0.73% |
| Equivalent | LQR | 3.43 | 3.56 | - |
| | PSO | 2.24 | 3.46 | 2.8% |
| | GWO | 2.23 | 3.45 | 3.1% |
| Variable | LQR | 3.43 | 3.56 | - |
| | PSO | 1.12 | 3.43 | 3.7% |
| | GWO | 1.11 | 3.42 | 3.9% |

Table V shows the comparison between the variance value of SOC, fuel consumption, and fuel savings using LQR, PSO, and GWO as the solver of the MPC framework with three different prediction steps. The variance of SOC provides information about the variation of the system state. In all cases, MPC with using an LQR solver has the highest variance value of SOC, indicating a higher variability in its results. The fuel consumption of the REEV using the LQR-driven

TABLE VI
FUEL CONSUMPTION AND SOC VARIANCE UNDER DIFFERENT INITIAL CONDITIONS

| Initial SOC | Target SOC | Fuel used (L/100kM) | Variance of SOC ($\times 10^{-6}$) |
|---|---|---|---|
| 0.20 | 0.20 | 3.80 | 3.86 |
| 0.40 | 0.20 | 3.45 | 3.52 |
| 0.60 | 0.20 | 3.06 | 3.18 |
| 0.80 | 0.20 | 2.63 | 2.77 |

Note: The variance of SOC is calculated starting when the SOC first reaches the target

MPC approach is selected as the baseline to compare with PSO-driven and GWO-driven MPC approaches. With using GWO as the solver of the variable-step prediction MPC framework, the studied REEV has the lowest fuel consumption (L/100kM), which saves 3.90% in compared with using the LQR as the solver, and 0.20% compared with using PSO. Under using the GWO as the solver in the MPC framework, the REEV using variable prediction step MPC approach has the lowest fuel consumption (L/100kM), which saves 3.17% compared with none prediction MPC approach and 0.8% compared to using equivalent step MPC approach.

Table VI presents the fuel consumption and SOC dynamics under various initial SOC to target SOC conditions. To ensure that the battery reaches the target SOC, all driver data were concatenated to establish a 3000-second driving cycle. It is observed that the higher the initial SOC, the lower the fuel consumption of the REEV, primarily because there is a period where the battery predominantly discharges before reaching the target SOC. Additionally, the variance of SOC after stabilization also shows a similar decreasing trend, reflecting the longer duration required for battery discharging, especially evident during the discharge from 0.8 to 0.2. Overall, all SOC variances are very small, indicating minimal variability in SOC once the target SOC is reached.

## VI. CONCLUSION

This paper leverages an experience-shared approach to variable-step predictive control to improve range-extended electric vehicles (REEV) energy efficiency. The performance has been comprehensively evaluated through a driver-in-the-loop co-simulation platform. The comparative study includes the performance of a transferable driver model, different prediction steps in model predictive control (MPC), and vehicle system robustness using different solvers in MPC.

1) The proposed experience-shared variable-step predictive control approach has been validated that have the ability to achieve the variable-step predictive control.
2) The transferable driver model has the lowest mean RMSE at 300 sample sizes when using transfer learning (3.08), compared to Gaussian mixed regression (GMR) with target driver data (29.4) and GMR with both source and target driver data (4.82).
3) In the vehicle system robustness, the violin plot shows that the distribution of the state of charge (SOC) values becomes more concentrated and the distribution of fuel consumption becomes lower as the prediction step length increases. The proposed variable-step MPC approach breaks this pattern and achieves the lowest fuel consumption.
4) Under the variable-step MPC frame, compared to using LQR as the solver, fuel consumption savings of 3.7% (L/100kM) were achieved by particle swarm optimization, and 3.9% (L/100kM) by grey wolf optimization (GWO).

The proposed experience-shared variable-step MPC approach has the potential to be deployed in various levels of automotive applications, such as battery management systems. External factors such as weather and altitude can be integrated into the transferable driver model for more accurate speed prediction.

## ACKNOWLEDGMENT

The authors would like to thank Birmingham CASE Automotive Research and Education Centre. They also would like to thank AVL List GmbH (AVL) for providing access to its advanced simulation technologies and software technical support within the frame of the University Partnership Program.

## REFERENCES

[1] D. T. Machacek, S. van Dooren, T. Huber, and C. H. Onder, "Learning-based model predictive control for the energy management of hybrid electric vehicles including driving mode decisions," *IEEE Trans. Veh. Technol.*, vol. 73, no. 4, pp. 5113–5127, Apr. 2024.

[2] H. Liu, Y. Lei, Y. Fu, and X. Li, "A novel hybrid-point-line energy management strategy based on multi-objective optimization for range-extended electric vehicle," *Energy*, vol. 247, May 2022, Art. no. 123357.

[3] Y. Sun, C. Xia, and J. Han, "Optimization of energy saving and fuel-cell durability for range-extended electric vehicle," *J. Energy Eng.*, vol. 149, no. 1, Feb. 2023, Art. no. 04022056.

[4] J. Li, Q. Zhou, H. Williams, H. Xu, and C. Du, "Cyber-physical data fusion in surrogate-assisted strength Pareto evolutionary algorithm for PHEV energy management optimization," *IEEE Trans. Ind. Informat.*, vol. 18, no. 6, pp. 4107–4117, Jun. 2022.

[5] J. Li et al., "Pedestrian-aware supervisory control system interactive optimization of connected hybrid electric vehicles via fuzzy adaptive cost map and bees algorithm," *IEEE Trans. Transport. Electrific.*, vol. 8, no. 2, pp. 2959–2970, Jun. 2022.

[6] J. Li, K. Liu, Q. Zhou, J. Meng, Y. Ge, and H. Xu, "Electrothermal dynamics-conscious many-objective modular design for power-split plug-in hybrid electric vehicles," *IEEE/ASME Trans. Mechatronics*, vol. 27, no. 6, pp. 4406–4416, Dec. 2022.

[7] Y. Zhang et al., "Predictive equivalent consumption minimization strategy based on driving pattern personalized reconstruction," *Appl. Energy*, vol. 367, Aug. 2024, Art. no. 123424.

[8] J. Li, Q. Zhou, H. Williams, and H. Xu, "Back-to-back competitive learning mechanism for fuzzy logic based supervisory control system of hybrid electric vehicles," *IEEE Trans. Ind. Electron.*, vol. 67, no. 10, pp. 8900–8909, Oct. 2020.

[9] J. Li, Q. Zhou, Y. He, H. Williams, H. Xu, and G. Lu, "Distributed cooperative energy management system of connected hybrid electric vehicles with personalized non-stationary inference," *IEEE Trans. Transport. Electrific.*, vol. 8, no. 2, pp. 2996–3007, Jun. 2022.

[10] D. Xu, C. Zheng, Y. Cui, S. Fu, N. Kim, and S. W. Cha, "Recent progress in learning algorithms applied in energy management of hybrid vehicles: A comprehensive review," *Int. J. Precis. Eng. Manuf.-Green Technol.*, vol. 10, no. 1, pp. 245–267, Jan. 2023.

[11] W. Golebiewski, K. Prajwowski, K. Danilecki, M. Lisowski, and K. F. Abramek, "Reducing the fuel consumption of an hybrid electric vehicle with the use of model predictive control–case study," *IEEE Trans. Veh. Technol.*, vol. 72, no. 9, pp. 11458–11468, Sep. 2023, doi: 10.1109/TVT.2023.3266829.

[12] T. Yuan and R. Zhao, "LQR-MPC-based trajectory-tracking controller of autonomous vehicle subject to coupling effects and driving state uncertainties," *Sensors*, vol. 22, no. 15, p. 5556, Jul. 2022.

[13] Ü. Önen, A. Çakan, and I. Ilhan, "Performance comparison of optimization algorithms in LQR controller design fora nonlinear system," *TURKISH J. Electr. Eng. Comput. Sci.*, vol. 27, no. 3, pp. 1938–1953, May 2019.

[14] M. Manimaran, S. Nagalakshmi, S. Vasanthi, and N. Muthukumar, "Evolutionary algorithm-based model predictive control for a reactive distillation column in biodiesel production," *Automatika*, vol. 64, no. 3, pp. 613–621, Jul. 2023.

[15] H. Yektamoghadam, A. Nikoofard, M. Behzadi, M. Khosravy, N. Dey, and O. Witkowski, "Multi-criteria evolutionary optimization of a traffic light using genetics algorithm and teaching-learning based optimization," *Expert Syst.*, vol. 41, no. 2, Feb. 2024, Art. no. e13487.

[16] J. Li et al., "Dual-loop online intelligent programming for driver-oriented predict energy management of plug-in hybrid electric vehicles," *Appl. Energy*, vol. 253, Nov. 2019, Art. no. 113617.

[17] H. He, Y. Wang, R. Han, M. Han, Y. Bai, and Q. Liu, "An improved MPC-based energy management strategy for hybrid vehicles using V2 V and V2I communications," *Energy*, vol. 225, Jun. 2021, Art. no. 120273.

[18] A. S. Hameed, H. M. B. Alrikabi, A. A. Abdul-Razaq, Z. H. Ahmed, H. K. Nasser, and M. L. Mutar, "Appling the roulette wheel selection approach to address the issues of premature convergence and stagnation in the discrete differential evolution algorithm," *Appl. Comput. Intell. Soft Comput.*, vol. 2023, pp. 1–16, May 2023.

[19] N. Moradi, V. Kayvanfar, and M. Rafiee, "An efficient population-based simulated annealing algorithm for 0–1 knapsack problem," *Eng. Comput.*, vol. 38, no. 3, pp. 2771–2790, Jun. 2022.

[20] S. Mirjalili, S. M. Mirjalili, and A. Lewis, "Grey wolf optimizer," *Adv. Eng. Softw.*, vol. 69, pp. 46–61, Mar. 2014.

[21] X. Li, D. Wu, J. He, M. Bashir, and M. Liping, "An improved method of particle swarm optimization for path planning of mobile robot," *J. Control Sci. Eng.*, vol. 2020, pp. 1–12, May 2020.

[22] M. Elsisi, "Improved grey wolf optimizer based on opposition and quasi learning approaches for optimization: Case study autonomous vehicle including vision system," *Artif. Intell. Rev.*, vol. 55, no. 7, pp. 5597–5620, Oct. 2022.

[23] S. Yang, W. Wang, and J. Xi, "Leveraging human driving preferences to predict vehicle speed," *IEEE Trans. Intell. Transp. Syst.*, vol. 23, no. 8, pp. 11137–11147, Aug. 2022.

[24] J.-H. Kim et al., "Modeling of driver's collision avoidance maneuver based on controller switching model," *IEEE Trans. Syst., Man Cybern., B Cybern.*, vol. 35, no. 6, pp. 1131–1143, Dec. 2005.

[25] J. Li, Q. Zhou, Y. He, H. Williams, and H. Xu, "Driver-identified supervisory control system of hybrid electric vehicles based on spectrum-guided fuzzy feature extraction," *IEEE Trans. Fuzzy Syst.*, vol. 28, no. 11, pp. 2691–2701, Nov. 2020.

[26] T. Taniguchi, S. Nagasaka, K. Hitomi, N. P. Chandrasiri, T. Bando, and K. Takenaka, "Sequence prediction of driving behavior using double articulation analyzer," *IEEE Trans. Syst. Man, Cybern. Syst.*, vol. 46, no. 9, pp. 1300–1313, Sep. 2016.

[27] A. Kesting and M. Treiber, "Calibrating car-following models by using trajectory data: Methodological study," *Transp. Res. Rec., J. Transp. Res. Board*, vol. 2088, no. 1, pp. 148–156, Jan. 2008.

[28] L. Alzubaidi et al., "A survey on deep learning tools dealing with data scarcity: Definitions, challenges, solutions, tips, and applications," *J. Big Data*, vol. 10, no. 1, p. 46, Apr. 2023.

[29] Y. Liu et al., "Imbalanced data classification: Using transfer learning and active sampling," *Eng. Appl. Artif. Intell.*, vol. 117, Jan. 2023, Art. no. 105621.

[30] C. Lu, F. Hu, D. Cao, J. Gong, Y. Xing, and Z. Li, "Transfer learning for driver model adaptation in lane-changing scenarios using manifold alignment," *IEEE Trans. Intell. Transp. Syst.*, vol. 21, no. 8, pp. 3281–3293, Aug. 2020.

[31] Z. Li, J. Gong, C. Lu, and J. Xi, "Importance weighted Gaussian process regression for transferable driver behaviour learning in the lane change scenario," *IEEE Trans. Veh. Technol.*, vol. 69, no. 11, pp. 12497–12509, Nov. 2020.

[32] M. Müller, "Dynamic time warping," in *Information Retrieval for Music and Motion*. Berlin, Germany: Springer, 2007, pp. 69–84. doi: 10.1007/978-3-540-74048-3_4.

[33] C. Wang and S. Mahadevan, "Manifold alignment using Procrustes analysis," in *Proc. 25th Int. Conf. Mach. Learn. (ICML)*, 2008, pp. 1120–1127.

[34] D. A. Reynolds et al., "Gaussian mixture models," *Encyclopedia Biometrics*, vol. 741, pp. 659–663, 2009.

[35] Y. Zheng, S. E. Li, K. Li, F. Borrelli, and J. K. Hedrick, "Distributed model predictive control for heterogeneous vehicle platoons under unidirectional topologies," *IEEE Trans. Control Syst. Technol.*, vol. 25, no. 3, pp. 899–910, May 2017.

[36] M. Ghalambaz, R. J. Yengejeh, and A. H. Davami, "Building energy optimization using grey wolf optimizer (GWO)," *Case Stud. Thermal Eng.*, vol. 27, Oct. 2021, Art. no. 101250.

[37] V. K. Kamboj, S. K. Bath, and J. S. Dhillon, "Solution of non-convex economic load dispatch problem using grey wolf optimizer," *Neural Comput. Appl.*, vol. 27, no. 5, pp. 1301–1316, Jul. 2016.

**Ji Li** (Member, IEEE) received the Ph.D. degree in mechanical engineering from the University of Birmingham, U.K., in 2020. He is currently an Assistant Professor of control and automation, the Deputy Head of the CASE Automotive Group, and the Manager of the Birmingham CASE Automotive Research and Education Centre, University of Birmingham. His research vision centralizes the critical role of artificial intelligence in shaping the future of automotive technology. Within this framework, the focus covers three key domains: multi-objective control, human–machine interaction, and cyber-physical systems, all oriented toward achieving net-zero and trustworthy engineering solutions. His work has gained international recognition on many occasions, including over 30 journal articles, two book chapters, and three best paper awards at well-known international conferences.

**Zirui Li** (Student Member, IEEE) received the B.S. degree from Beijing Institute of Technology (BIT), Beijing, China, in 2019, where he is currently pursuing the Ph.D. degree in mechanical engineering. From June 2021 to July 2022, he was a Visiting Researcher with Delft University of Technology (TU Delft). Since August 2022, he has been a Visiting Researcher with the Chair of Traffic Process Automation, Faculty of Transportation and Traffic Sciences "Friedrich List," TU Dresden. His research interests include interactive behavior modeling, risk assessment, and the motion planning of automated vehicles.

**Chengqing Wen** received the B.S. degree in electronics and information engineering from Xidian University, Xi'an, China, in 2020, and the M.Sc. degree in electronic and computer engineering from the University of Birmingham (UoB), Birmingham, U.K., in 2021, where he is currently pursuing the Ph.D. degree with the Connected and Autonomous Systems for Electrified Vehicles (CASE-V) Team. His research interests include energy management systems for hybrid electric vehicles and data-driven modeling for powertrain systems.

**Yanhong Wu** received the M.S. degree in vehicle engineering from Chongqing Jiaotong University, Chongqing, China, in 2020. He is currently pursuing the Ph.D. degree with the School of Electrical Automation and Information Engineering, Tianjin University, Tianjin, China. He is a Visiting Student with the University of Birmingham, U.K. His research interests include surrogate-driven modeling, model predictive control, and their applications on connected and autonomous vehicles.

**Roger Dixon** received the B.Eng. degree (Hons.) in mechanical engineering and the M.Sc. degree in mechatronics from Lancaster University in 1992 and 1993, respectively, and the Ph.D. degree in discrete time modeling and control from the Centre for Research in Environmental Systems and Statistics (CRES) in 1996. He is currently a Professor of control system engineering with the University of Birmingham, Birmingham, U.K., where he is also the Director of Birmingham Centre for Railway Research and Education. He is a Specialist in applied control systems, mechatronics, condition monitoring, fault detection, and systems engineering. He has published over 150 research articles and has led major research activities in industry and academia.

**Xiaosong Hu** (Fellow, IEEE) received the Ph.D. degree in automotive engineering from Beijing Institute of Technology, Beijing, China, in 2012. From 2010 to 2012, he completed his scientific research and Ph.D. dissertation with the Automotive Research Center, University of Michigan, Ann Arbor, MI, USA. He is currently a Professor with the College of Mechanical and Vehicle Engineering, Chongqing University, Chongqing, China. His research interests include modeling and control of alternative powertrains and energy storage systems.

**Hongming Xu** received the Ph.D. degree from Imperial College London in 1995. Then, he was a Research Fellow and a Senior Research Fellow with Imperial College London. He moved to Jaguar Cars Ford Premier Automotive Group in 2000, where he was a Project Engineer (2000–2001), a Team Leader (2002–2004), and a Principal Technical Specialist. Then, he joined the University of Birmingham as a Reader of automotive engineering in 2005. He is currently a Professor of energy and automotive engineering with the University of Birmingham, Birmingham, U.K., where he is also the Head of the Vehicle and Engine Technology Research Centre. He has authored or co-authored over 400 journals and conference publications on advanced vehicle powertrain systems. He is a fellow of SAE and IMechE.